Austin Journal of Nanomedicine & Nanotechnology

Austin Publishing Group

Open Access Full Text Article

Research Article

Long Circulating Nanoparticles as Potential Antigen Carriers in Angiogenic Blood Vessels: Towards Tolerogenesis

Amy Tekrony[1], Vincent Wright[2], Anne Slaney[2], Usama Al-Atar[2], Amy Frederick[1], Teresa Rodriguez[1], Jillian Buriak[2], David Cramb[1,4]* and Lori West[3]

[1]Department of Chemistry, University of Calgary, Canada
[2]Department of Chemistry, University of Alberta, Canada
[3]Departments of Pediatrics, Surgery, and Immunology, University of Alberta, Canada

***Corresponding author:** David Cramb, Department of Chemistry, University of Calgary, 2500 University DR NW, Calgary, AB T2N 1N4, Canada, E-mail: dcramb@ucalgary.ca

Received: November 27, 2013; Accepted: December 23, 2013; Published: December 31, 2013

Abstract

Infants do not produce typical immune responses to foreign ABO-blood group antigens compared to older individuals who have a fully developed immune system. Therefore, incompatible donor organs can be transplanted into infants without rejection, which results in immunological tolerance. As a result, we hypothesized that intentional introduction of ABO-antigens would also induce tolerance and extend the period of time for safe ABO- incompatible transplantations. A proposed method to induce tolerance is by conjugating antigens to long-circulating silica nanoparticles and injecting them into blood vessels to promote maximum exposure of lymphocytes to the antigens. Here, we characterized synthesized nanoparticles for this purpose. Nanoparticle brightness and aggregation tendencies were determined for detectability and stability in a living system, respectively, using fluorescence correlation spectroscopy. Bright, non-aggregating nanoparticles were injected into the chorioallantoic membrane of chicken embryos to monitor circulation. It was determined that 100 – 200nm PEG-coated silica nanoparticles were easily detected, aggregated little, and circulated for a prolonged period of time in the blood stream.

Keywords: Silica nanoparticles; Tolerogenesis; Stealth nanoparticles; Fluorescence correlation spectroscopy; Chorioallantoic membrane of the chicken embryo

Introduction

It has been known for many years that induction of antigen tolerance is possible in animals. In 1945, Owen defined the inherent susceptibility that animals have to immune tolerance [1]. In 1949, Burnet and Fenner linked this tolerance to developmental events, using twin fetal cows [2], and in 1953, Medawar showed that this tolerance could be induced intentionally in mice [3]. Up until now, these findings were not considered to be clinically relevant to humans since human neonates have an increased maturity of their immune systems at birth in comparison to animals, and therefore were thought to be beyond susceptibility to tolerance induction. A study by West and co-workers showing successful incompatible heart transplants was the first to refute what was previously thought and provide evidence for neonatally acquired donor-specific blood type antigen immune tolerance in humans [4]. Fan et al. also provide evidence that suggests persistent exposure to donor antigens is required for tolerogenesis (induction of immune tolerance), which is dependent on the degree of antigen expression [5]. Since evidence shows that the occurrence of tolerogenesis is dependent on degree of antigen exposure, it may be possible to induce tolerance via methods other than graft exposure or transplantation, thereby possibly reducing mortality rates on transplantation wait lists. If an infant must wait for an organ past the time of susceptibility to induced tolerance, it may beneficial to induce that tolerance previously to allow for tolerance to both A and B antigens, or essentially make that infant's blood type a "universal acceptor". This would increase the likelihood of transplantation at a later point in time when a donor organ may be available, thereby decreasing the likelihood of a fatal outcome.

In order to achieve this goal, it is essential to determine novel methods of tolerance induction. Since lone antigens in the blood stream would likely be cleared quickly by the renal system, our study takes steps towards the possibility of injecting nanoparticle-antigen conjugates into the blood stream to induce tolerance. Ideal particles will be easily detected and circulate for a prolonged period of time in vasculature to ensure maximum exposure to blood stream antigens. Therefore, since polyethylene glycol (PEG) coatings have been shown to increase nanoparticle (NP) circulation time in the blood stream, the majority of the silica NPs in this study were functionalized on their surfaces with PEG [6]. Silica has demonstrated biocompatibility [7] and silica NPs are easily tuned for size [8]. In addition, most NPs synthesized contain fluorescent dyes for detection in order to monitor and assess their localization and circulation behaviour.

Previous NP circulation studies have been performed either in adult animals [9] or in tumor models [10]. Neither of these are the most relevant to model neonatal blood circulation. Neonates will have varying degrees of natural angiogenesis, which is poorly represented by tumor models and not at all by adult animals. Desirable is a simple angiogenic model into which NPs can be injected and tracked for circulation time, aggregation behavior and general stability. The chorioallantoic membrane (CAM) of the chicken embryo is an

Citation: Cramb D , Wright V, Slaney A, Al-Atar U, Frederick A, et al. Long Circulating Nanoparticles as Potential Antigen Carriers in Angiogenic Blood Vessels: Towards Tolerogenesis. Austin J Nanomed Nanotechnol. 2013;1(1): 1005.

excellent model for angiogenesis. Within the CAM the blood pressure is normal and the vessels are not tortuous unlike tumor models and those of most of the blood vessels in the zebrafish embryo. The CAM serves as the respiratory system for the chicken embryo up until day 19 of the 21 day gestation period, handles any waste products from the embryo, and supplies the embryo with nutrients from the yolk [11], The CAM has been used as a model to study angiogenesis of explanted tumors and anti-angiogenic drugs [12-18], tumor vascular targeting [19], metastasis [20,21], ion transport [22], allergens [23], transplantation [24], contraceptives [25,26], effects of hyperglycemia [27], and photodynamic therapy [28]. NPs can easily be injected into blood vessels of the CAM through a window cut into the eggshell, and it has been shown that the concentration of certain particles decreases exponentially within the first few minutes of injection [29,30]. This is due to loss of the NPs from the blood stream through the angiogenic fenestrations (~500nm in size) [31]. The presence of angiogenesis in these developing vessels allows us to find ideal NPs that will circulate for a prolonged period of time, despite the "leaky" nature of the developing vessels. The NP concentration in the CAM can be monitored through the window in the shell using fluorescence correlation spectroscopy (FCS).

Two-photon excitation (TPE) -FCS is a non-invasive fluorescence technique commonly used to analyze fluorescent particles in living organisms, primarily for advantages such as: low phototoxicity, long-term analysis and ability to distinguish aggregation [29]. TPE-FCS involves analysis of fluorescent intensity fluctuations resulting from two-photon excitation of fluorescent molecules to obtain data about diffusion, concentration, and size of the fluorophores. TPE-FCS has been used to gain valuable information in many applications such as the examination of angiogenic blood vessel formation in zebrafish; the study of active transport, localization of proteins, and diffusion of receptor clusters in cells; monitoring drug delivery using photocages; and the study of DNA replication [32].

In this study, TPE-FCS is used as the primary technique to provide minimally invasive monitoring of NP behaviour in the CAM of the chicken embryo. By tracking the change in concentrations and aggregation tendencies as functions of size and surface chemistries, we may determine which NPs are most easily detected, aggregate the least, and circulate in the blood stream the longest. These data will allow us to predict the NP properties most suitable to provide maximum blood exposure to the synthesized antigens used to induce immunological tolerance in infants.

Methods

Nanoparticle design and synthesis

Various NPs were synthesized with a range of: dyes, ratios of dye to silica, surface functionalizations, and dye-incorporation methods (See Table 1 for the naming system for nanoparticles, according to their synthesis). NPs with dye incorporation were synthesized according to the Stöber process [33], which involves the hydrolysis of alkyl silicates, followed by the condensation of silica acid in alcohol using ammonia as a catalyst. This synthesis resulted in uniform particles of which sizes can be controlled from approximately 50nm to 2000nm in diameter [33]. In order to synthesize the core-shell particles, a modified version of the Stöber process was used, as described by Larson et al. [34], in which the dye-rich compact core is synthesized prior to the silica shell. The NPs were functionalized by directly adding polyethylene glycol (PEG) or (3-aminopropyl) -trimethoxysilane (APTMS) to the synthesis flask, which formed covalent bonds from the polymers to the NPs as the base-catalyzed silanization occurs [35]. Once synthesized, particles were resuspended in water and stored in scintillation vials covered with aluminum foil to reduce exposure to light.

Two-photon excitation fluorescence correlation spectroscopy

As the name suggests, TPE utilizes the energy from two photons to promote a molecule into an excited state. The TPE energy is at least half the one-photon excitation (OPE) energy, resulting in the need of the molecule to absorb two photons simultaneously in order to reach an excited state. Since the absorption of two photons is less probable than the absorption of one photon, TPE results in a smaller excitation volume and thus increases the precision of the laser beam. A higher density of photons and thus a higher power is used for excitation without the need to increase the energy and cause photothermal damage. Since the probability of a transition into the excited state is proportional to the square of the instantaneous light intensity, the focal volume is reduced to a smaller focal volume confined to three-dimensions unlike that from OPE. This is extremely advantageous when exciting in biological samples as excitation to surrounding tissue is minimized and thus so is the overall photodamage. The lower energy of light needed for this process also allows for less damage to surrounding tissue.

TPE-FCS measures the fluctuations of fluorescence in an optically-defined interrogation volume over time. A temporal autocorrelation analysis is performed on the fluorescence intensity data (see Figure 1) to generate the autocorrelation decay, G (t) [36].

$$G(\tau) = \frac{\langle \partial F(t) * \partial F(t+\tau) \rangle}{\langle F \rangle^2} \quad (1)$$

Where ∂F(t) is the difference between the instantaneous fluorescence at time, t, and the average fluorescence intensity, $\langle F \rangle$. As the lag time, τ, increases, $G(\tau)$ decreases, and an autocorrelation decay

Material		Functionalization		Dye Incorporation		Dye	
Symbol	Meaning	Symbol	Meaning	Symbol	Meaning	Symbol	Meaning
Si	Silica	PEG	Polyethylene glycol	R	Random	R6G	rhodamine 6G
Fe	Iron oxide	NR_3	Amine	C	Core-shell	TRITC	tetramethyl isothiocyanate
		SPEG	Short PEG	NP	Lg NPs from sm NPs	FITC	fluorescein isothiocyanate
		LPEG	Long PEG			AFX	Alexa Fluor®
		NF	No Funct.			Pyr	Pyrene-maleimide

Table 1: Symbols used for naming nanoparticles.

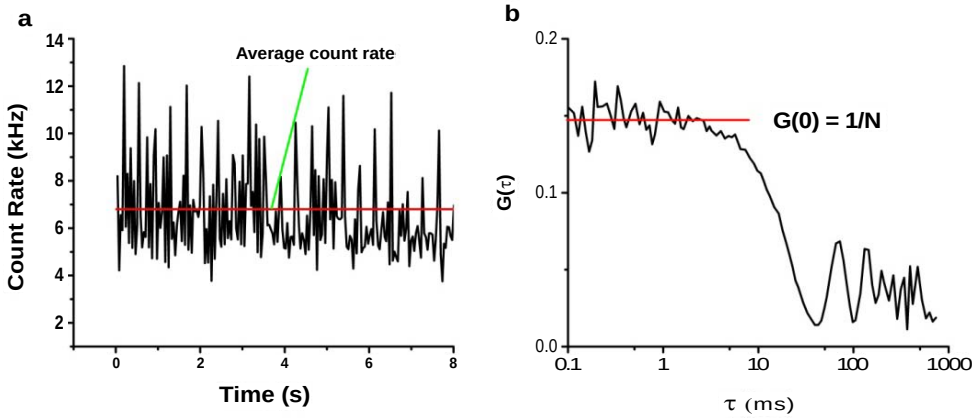

Figure 1: a) Count rate fluorescence trajectory, where the red line is equal to the average count rate and b) Autocorrelation decay curve, where the red line depicts G(0), which is equal to 1/N. Both graphs are examples of typical plots that result from FCS analysis of nanoparticle injection into the CAM.

(ACD) curve results. Equation (2) can be used to model the ACD, when the system is dominated by Brownian diffusion determine the diffusion coefficient, size, and concentration of the NPs [37].

$$G(\tau)=\frac{\left[1+\frac{\left(\frac{\tau}{1000}\right)8D}{r^2}\right]^{-1}\left[1+\frac{\left(\frac{\tau}{1000}\right)8D}{Z_0^2}\right]^{-\frac{1}{2}}}{\langle c\rangle\left(\frac{\pi}{2}\right)^{\frac{3}{2}}r^2Z_0} \quad (2)$$

Where r is the radius of the ovoid of the two photon excitation volume (perpendicular to the direction of laser propagation), Z_0 is the depth of the ovoid of two photon excitation (in the direction of laser propagation), c is the local concentration, D is the diffusion coefficient, and is the lag time. It is also important to note from Equation 2 that G(0) is equal to 1/<N> (where<N>equals the average number of freely diffusing fluorescent particles in the TPE volume). Thus, <N> is the equivalent of concentration. Changes in <N> over time may indicate the NPs are being taken up into the angiogenic tissue, aggregating or dissolving.

To help determine the origin of NP concentration changes we will use the average particle brightness, η. If <N> decreases and η increases, this suggests aggregation is taking place. If <N> decreases and η remains constant, this suggests uptake or dissolution. And finally if <N> remains constant and η decreases this suggests that the fluorescent dye in the NPs is unstable, which could indicate that the NP surfaces are changing. It is simple to calculate the particle brightness (kHz/NP):

$$\eta = 1/\langle N\rangle * \langle F\rangle \quad (3)$$

For all experiments, count rate trajectories and autocorrelation decay curves were plotted and analyzed using OriginPro 7.

Nanoparticle characterization in solution

In order to assess the suitability of the NPs for injection into the CAM, initial characterization of the NP solutions was first performed in various solutions. If the NPs were unstable in simple solution, they were deemed inappropriate for study in the CAM environment. Particles were diluted to the 10-100 nM concentration range (10 <<N>< 100). This would be the appropriate range for the CAM studies and likely the desirable range for tolerogenesis. Particles that were monodisperse, bright, and gave consistent autocorrelation decay curves in water, were further analyzed in various buffer and sera solutions.

The monodisperse, bright NPs mentioned above were analyzed for their behaviourin phosphate buffered saline (PBS), chicken blood serum (CBS), and porcine blood serum (PorBS) over time to observe possible effects on salts and proteins on the NPs from the buffer and sera, respectively on brightness and aggregation. FCS measurements were taken at short intervals for the first 30 minutes post dilution and at longer intervals after that over the time span of an hour. Autocorrelation decay curves and count rate trajectories were analyzed for signs of aggregation, changing concentration, changes in particle brightness.

CAM preparation

Fertilized eggs were obtained from the Ijtsma Poultry Farm north of Calgary (RR 284 and highway 72, Mailing address: RR2, Site 11, Box 6, Airdrie, AB, T4B 2A4). Eggs were stored for up to two weeks in a refrigerator at 4°C, at which time they lose viability. The details of the CAM preparation have been described previously [38]. Briefly, nine days before experimentation, eggs were removed from the refrigerator and allowed to sit at room temperature for a few hours. The eggs were then incubated at 37 degrees Celsius and approximately 60% humidity. On day four and a half of the incubation period, the eggs were windowed to provide visual observation of the embryo development [38]. Cellulose tape was then used to cover the window in the egg, and the eggs were placed back into the incubator. Over the course of the subsequent incubation period, embryos were monitored. On day nine of incubation, the eggs were removed once again for experimentation. The windows in the eggs were expanded to allow for injection of nanoparticles and monitoring of the injectate via FCS. The top portions of the eggs were further covered with cellulose tape to prevent crumbling of the shell into the amniotic fluid and CAM. Dissecting scissors were then used to cut the shell away to the line of the fluid within the egg, thus providing maximum exposure to the

CAM for experimentation.

S2.4. Microinjection

Injections were performed using a manual microinjector from Sutter Instruments Co. Needles were formed using P-30 Puller (Sutter Instruments Co.), beveled using a K. T. Brown Type Micro-Pipette Beveller, Model BV-10 (Sutter Instruments Co.), and held in place and directed by an x, y, z-manipulator (Sutter Instruments Co. , MM-33).

Undiluted nanoparticles were drawn up into a 3 mL BD syringe, which was then attached to the top of the microinjector. The tubing that leads to the manipulator was primed, and a beveled needle was secured into place at the end of the tubing. The needle was also primed and flow through the tip was verified. The valve leading from the BD syringe port to the micro syringe was opened and nanoparticles were drawn into the micro syringe.

Once the microinjecter was set up, an egg was placed in an egg holder on the egg stage of the microscope (In-house design, University of Calgary, [38]) and viewed through the 5X objective with a 1 cm working distance. The needle, adjusted to inject parallel to blood flow. Approximately 100 µL of nanoparticles were then injected into CAM blood vessels of approximately 100 – 200 µm in diameter.

After successful injections, the objective turret position was changed to the 20X lens and the laser was focused in the center of the blood vessel. The focused laser beam was always several hundred microns downstream from the injection site.

Chicken Embryo Chorioallantoic Membrane (CAM) Model for Nanoparticle Characterization

NPs that did not aggregate in solution and were bright enough to be easily detected were injected into blood vessels of the CAM. The NPs were injected through a window of a chicken embryo egg into the blood vessels of the CAM, which are contiguous with the vessel system in the embryo, and FCS was used to track concentration changes of the NPs within the blood vessels. More precisely, 100 µL of undiluted NP solution was injected into a vessel of approximately 100 to 200 µm in diameter. The injectate was allowed to circulate and distribute throughout the blood stream (30 s, [29]), after which FCS measurements were taken continuously from approximately 3 min post injection to approximately 50 min post injection, with the TPE laser beam focused into the center of the lumen.

S2.5. Zeta-Potential Measurement

Nanoparticles were diluted to approximately 10^{-10} M concentration from original solutions, and a small amount was drawn into a 3 mL BD syringe. Nanoparticles were then injected into disposable polystyrene cuvettes and inserted into the cell holder in the Nano ZS DLS instrument (Malvern Instruments Ltd). Zeta-potentials were obtained in water using averaged data from approximately 80 accumulated data points and pre-assigned settings for silica nanoparticles with the refractive index set to 1.5, the refractive index of silica.

Results and Discussion

Nanoparticlestability in aqueous solution and blood sera

A series of approximately 50 types of NPs that were synthesized with various combinations of sizes, dyes, surface functionalizations, polymer materials, and synthesis methods, were analyzed for stability in aqueous solution and blood sera. The key findings for aqueous solution are presented in Table 2, which gives average particle brightness, the percentage of particles that aggregated, and were used in eggs. All these are categorized based on particle synthetic variables. To sleuth out trends in the characteristics of the NPs, all data for specific characteristics were pooled and then the averages or % displaying the behaviour were calculated. For example, 46 types of NPs were surface-functionalized with PEG. Their cumulative average $\eta$was 3.5 kHz per particle, 13/46 displayed aggregation in water and 11/46 wereultimately deemed suitable for further study in the CAM. Thus,the results displayed in Table 2 were used to help determine which NPs were stable and bright enough for use in the CAM *in vitro* studies.

Variable		η, average particle brightness (kHz/particle)	Percent of particles that aggregated in water	Percent injected into eggs (%)
NP Material	Iron oxide core	0	N/A	0
	Silica	3.2	36	23
Functionalization	PEG	3.5	28	23
	Amine	0.3	80	20
	None	1.3	100	0
Dye-incorporation Method	Core-shell	4.0	41	32
	Random	1.5	0	0
	Large particles made from small ones	0	75	0
Dye	Rhodamine 6G	4.4	32	29
	TRITC*& FITC§	1.1	33	16
	Alexa fluor	0.8	50	0
	Pyramine	0.2	50	0
Size	0-75nm	3.7	60	0
	75-200nm	3.9	30	37
	>200nm	0.8	25	8

Table 2: Summary of nanoparticle characterization results in water.
* tetramethyl isothiocyanate, § fluorescein isothiocyanate

Out of the fifty particle solutions investigated in water, twelve types of NPs were mixed with buffer and blood sera to further investigate stability in the presence of ions and proteins. Table 3 displays the results of these studies.

There was increased particle instability and aggregation in blood serum in comparison to buffer. This was also observed in a study by Eberbeck *et al.* , in which they studied magnetic particles in different solutions. It was found that particles had a higher tendency to aggregate in different biological media [39]. However, the results from mixing the silica NPs in different solutions were very promising as a large number of the NPs synthesized showed high stability in PBS and in two different blood sera, which was beneficial for the desired purpose of injecting them into the embryonic chicken CAM blood vessels.

Overall, seven out of the total of 50 NPs were deemed appropriate to be injected into the CAM model, which reflects the importance of the specific combination of variables on resulting particle properties. Interestingly, all of the particles that were determined to be suitable for injection were core-shell silica NPs; the core-shell particles tended to be brighter, thus more easily detected for the purposes of this study. All of the NPs injected into the eggs were those functionalized with PEG. Five were synthesized utilizing R6G as the dye, while the other two contained TRITC. Also, all NPs stable enough to be injected into the CAM had hydrodynamic diameters in between 89 to 250 nm.

Nanoparticles in the CAM

Based on the above-mentioned results, seven different NPs were studied in the CAM blood vessels. Out of those seven particle solutions, five were found to be stable in the CAM vasculature, with little signs of extensive aggregation over the time periods analyzed (30-60 min).

Figure 2a displays a typical plot of the number of silica NPs in the TPE volume, *N*, as a function of time for all of the particles injected into the CAM. As demonstrated in Figure 2a, there is no indication of any systematic change in particle numbers over the time period (33 min) for this particular NP. The large scatter in the data (average +/- 50%) (Figure 2a) results from a number of factors: inhomogeneities in the concentration in time due to pulsatile flow, movement of the embryo and some small degree of aggregation. Recall that the angiogenic blood vessels of the CAM possess fenestrations that are 500 nm in diameter or smaller [38]. Therefore, NPs smaller than this size could leave the blood stream through these nanofenestrations. Figure 2b, by comparison shows dioleoylphosphatidyl-serine (DOPS) liposomes (ζ=-59mV and 100 nm diameter) injected into the CAM. In the case of DOPS, there is clearly a slow decrease in *N* over time, which we have previously shown is due to uptake into the angiogenic blood vessel walls [31].

Nanoparticle	Approximate time in solution until aggregation is observed (min)		
	PBS	CBS	PorBS
Si_PEG_C_TRITC_89nm	>60	>16	Insufficient data
Si_PEG_C_R6G_105nm	>60	>60	24
Si_PEG_C_R6G_120nm	>60	>60	<6
Si_PEG_C_R6G_125nm	35	45	2
Si_PEG_C_R6G_142nm	>45	45	19
Si_PEG_C_R6G_148nm	>60	23	40
Si_PEG_C_R6G_150nm_2	10	9	<8
Si_PEG_C_R6G_177nm	>60	60	23
Si_PEG_R_TRITC_179nm	>60	15	8
Si_PEG_C_R6G_191nm	>45	45	40
Si_PEG_C_TRITC_250nm	Insufficient data	7	6
Si_PEG_R_R6G_350nm_2	20	11	<16

Table 3: Observed time of nanoparticle aggregation in various solvents over the typical 45 to 60 minutes of data collection, determined from CRT and ACD analysis.

The lack of verifiable uptake for these NPs in the CAM is quite significant, since this is not the case with most particles of similar sizes studied in the Cramb group. In our previous work, we found many different NPs that were taken up into the angiogenic tissues. These particles included PEGylated quantum dots, polystyrene fluospheres and liposomes [31]. It is emerging that size, functionalization, and surface potential all play a large role in the observed uptake rates. We have shown previously that uptake rates have been found to be

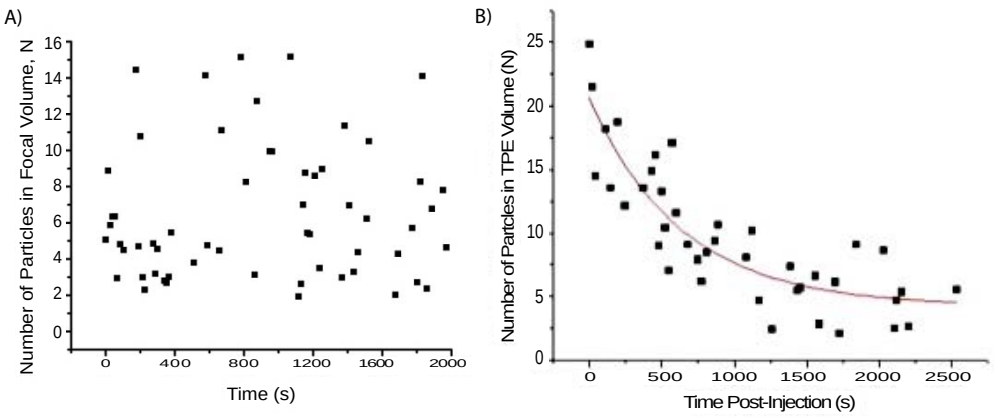

Figure 2: Number of particles in focal volume versus time post injection into eggs for a) 89 nm core-shell TRITC silica particles with PEG functionalization. b) 102 nm diameter DOPS liposomes loaded with lissamine. Red curve represents monoexponential decay fit with rate constant, k=0.002 s^{-1}.

dependent on size for particles with zeta potentials in the range 0<z <-40 mV [31]. The silica NPs in the current study are of similar sizes to these NPs, but do not deposit in the vessel walls. We therefore propose that there is a negative charge cut-off, which plays a significant role in keeping the NPs in the blood stream. This cut-off appears to be around -50 to -60 mV as discussed in [31], and shown in Table 4 as particles with high negative charges are not taken up readily. These finding are likely a result of the large negative zeta potentials of the NPs causing repulsion with the negatively charged endothelial cells making up the blood vessel walls. Furthermore, large surface charge could help to stabilize NPs as the NP-NP repulsion would reduce aggregation. Since many of the non-silica particles in our previous study that displayed uptake are coated with PEG and are of similar diameters [31], this charge effect is likely a significant reason for the differences in circulation behaviour. This result is also supported by the contrast in the results for the circulation behavior of liposomes. The zwitterionic dioleyolphosphatidyl-choline (DOPC, ζ = -40 mV, 100 nm diameter) left the blood stream with a rate constant of $k_{loss} = 0.003\ s^{-1}$ [31], whereas the DOPS liposomes (ζ = -59 mV, 100 nm diameter) lasted 50% longer in circulation, $k_{loss} = 0.002\ s^{-1}$ (Figure 2).The charge-induced, long circulation time is a very beneficial characteristic for tolerogen carriers, as it would permit maximum exposure of B-cells to NP-conjugated antigens.

Lack of uptake does not necessarily mean complete stability of the silica NPs during circulation. Some were observed to display a degree of aggregation after prolonged exposure to the CAM blood stream. Table 4 gives the length of time during circulation before aggregation of the NPs was observable and represents the onset of 20-25% aggregation of the NPs. From Table 4, it is evident that PEG-coated NPs in the size range 120-150 nm diameter were optimal for better stability against aggregation.

Other PEG-functionalized particles, similar to the silica NPs used in this study, have shown similarly long circulation times in other animal models. For example, Maldiney at al. studied the effects of diameter and surface coating on biodistribution within healthy mice [40]. As part of the study, the biodistribution of intravenously administered silicate-based NPs coated with PEG (chain length approximately 10 times longer than the ones use in this study) was compared to that of particles with exposed hydroxyl groups. It was found that PEG-functionalized particles circulated in mice for a longer period of time than the similar hydroxyl-functionalized particles [40]. This was indicated by the rapid uptake of the hydroxyl-coated particles into the liver and a high distribution of the PEG functionalized particle throughout the rest of the organism [40]. Maldiney also found a strong dependence on size with longer circulation times for particles with 120 nm hydrodynamic diameter compared with larger particles (190-230 nm) [40]. Interestingly, their study found that negatively charged, bare silica particles were rapidly deposited in the liver and spleen. We saw little evidence of this for the negative particles in the current study, however our particles did have a degree of PEG coating and the CAM blood volume is very large compared with the organ blood volume. It is also notable that the chicken embryo has an immature immune system at this incubation point [41]. Thus uptake by macrophages is limited in the CAM model.

Nanoparticle	Approximate time (post injection) until aggregation is observed (min)	ζ (SD, mV)
Si_PEG_C_TRITC_89nm	25	-64 (20)
Si_PEG_C_R6G_105nm	45	Insufficient data
Si_PEG_C_R6G_120nm	no aggregation	-60 (10)
Si_PEG_C_R6G_125nm	no aggregation	-47 (15)
Si_PEG_C_R6G_150nm_2	no aggregation	Insufficient data
Si_PEG_C_R6G_177nm	45	-68 (9)
Si_PEG_C_TRITC_250nm	30	-48 (5)
DOPS liposomes	no aggregation	-59 (12)

Table 4: Zeta potentials and observed time of nanoparticle aggregation in the CAM over the typical 45 to 60 minutes of data collection, determined from CRT and ACD analysis.

PEG has been validated in many previous studies as a coating that increases blood stream circulation time of NPs [42-45]. Our previously reported work has demonstrated that amino-terminated PEG coated quantum dots disappear too quickly from the CAM blood stream to measure the uptake rates (35). Intuitively, the amino functionalization would cause particles to be less negative and therefore be attracted to the negative endothelia cells of the CAM blood vessels. It therefore emerges that a combination of PEGylation and large, negative charge promote longer circulation time in angiogenic blood vessels.

Conclusion

PEGylated silica nanoparticles were studied in the CAM model as a significant step towards developing long-circulating, stable tolerogen carriers. Such NPs would allow for an increased exposure of the blood stream to the antigens they will carry. It was found that PEG-functionalized particles between 90 to 200 nm in diameter with large negative charges produced the desired effects and circulated for long periods of time in CAM blood vessels. PEGylated silica NPs reported in this work carry large negative charges likely because of incomplete coverage of the silica surface by PEG. These findings suggest that silica NPs with the above-mentioned qualities would be suitable for tolerogenesis. As a result, these silica NPs will be conjugated to antigens to determine if the resulting exposure will be persistent enough to induce immunological tolerance to foreign blood type antigens.

Acknowledgements

The authors would like to thank the Natural Sciences and Engineering Council of Canada and the Canadian Institutes of Health Research for their financial support.

References

1. Owen RD. Immunogenetic Consequences of Vascular Anastomoses Between Bovine Twins. Science. 1945; 102: 400-401.
2. Burnet FM, Fenner F. The Production of Antibodies. Melbourne, Australia: Macmillan and Co., Ltd.; 1949.
3. Billingham RE, Brent L, Medawar PB. Actively acquired tolerance of foreign cells. Nature. 1953; 172: 603-606.
4. West LJ. B-cell tolerance following ABO-incompatible infant heart transplantation. Transplantation. 2006; 81: 301-307.
5. Fan X, Ang A, Pollock-Barziv SM, Dipchand AI, Ruiz P, Wilson G, et al. Donor-specific B-cell tolerance after ABO-incompatible infant heart transplantation. Nat Med. 2004; 10: 1227-1233.

6. Rio-Echevarria IM, Selvestrel F, Segat D, Guarino G, Tavano R, Causin V, et al. Highly PEGylated silica nanoparticles: “ready to use” stealth functional nanocarriers. J Mater Chem. 2010; 20: 2780-2787.

7. Radu A, Eleonora C, Lucian A, Georgeta C, Virginia V, Cristiana T. *In vitro* biocompatibility testing of implantable biomaterials. Rom Biotech Lett. 2008; 13: 3863-3872.

8. Ow H, Larson DR, Srivastava M, Baird BA, Webb WW, Wiesner U. Bright and stable core-shell fluorescent silica nanoparticles. Nano Lett. 2005; 5: 113-117.

9. Almeida JP, Chen AL, Foster A, Drezek R. In vivo biodistribution of nanoparticles. Nanomedicine (Lond). 2011; 6: 815-835.

10. Jabir NR, Tabrez S, Ashraf GM, Shakil S, Damanhouri GA, Kamal MA. Nanotechnology-based approaches in anticancer research. Int J Nanomedicine. 2012; 7: 4391-4408.

11. Schlatter P, König MF, Karlsson LM, Burri PH. Quantitative study of intussusceptive capillary growth in the chorioallantoic membrane (CAM) of the chicken embryo. Microvasc Res. 1997; 54: 65-73.

12. Chen H, Wang CS, Li M, Sanchez E, Li J, Berenson A, et al. A novel angiogenesis model for screening anti-angiogenic compounds: the chorioallantoic membrane/feather bud assay. Int J Oncol. 2010; 37: 71-79.

13. Li YJ, Duan CL, Liu JX, Xu YG. Pro-angiogenic actions of Salvianolic acids on in vitro cultured endothelial progenitor cells and chick embryo chorioallantoic membrane model. J Ethnopharmacol. 2010; 131: 562-566.

14. Iurlova EI, Rubina KA, Sysoeva VIu, Sharonov GV, Semina EV, Parfenova EV, et al. [T-cadherin suppresses the cell proliferation of mouse melanoma B16F10 and tumor angiogenesis in the model of the chorioallantoic membrane]. Ontogenez. 2010; 41: 261-270.

15. Cimpean AM, Ribatti D, Raica M. The chick embryo chorioallantoic membrane as a model to study tumor metastasis. Angiogenesis. 2008; 11: 311-319.

16. Cimpean AM, Ribatti D, Raica M. The Chick Embryo Chorioallantoic Membrane as an In Vivo Model for Study Tumor Angiogenesis and Metastasis. Anticancer Res. 2008; 28: 118.

17. Richardson M, Liu L, Dunphy L, Wong D, Sun Y, Viswanathan K, et al. Viral serpin, Serp-1, inhibits endogenous angiogenesis in the chicken chorioallantoic membrane model. Cardiovasc Pathol. 2007; 16: 191-202.

18. Tufan AC, Satiroglu-Tufan NL. The chick embryo chorioallantoic membrane as a model system for the study of tumor angiogenesis, invasion and development of anti-angiogenic agents. Curr Cancer Drug Targets. 2005; 5: 249-266.

19. Willey CD, Burleson TM, Zhai L, Anderson JC. The Development of a Chorioallantoic Membrane-tumor Xenograft Model for Tumor Vascular Targeting with Radiation. Int J Radiat Oncol Biol Phys. 2010; 78: S624-S5.

20. Tan Q, Steiner R, Hilbe M, Hillinger S, Weder W, Lu S. Tissue engineered tumor cultured on chick embryo chorioallantoic membrane (CAM): a new model of spontaneous metastasis. J Thorac Oncol. 2009; 4: S639-S40.

21. Deryugina EI, Quigley JP. Chick embryo chorioallantoic membrane model systems to study and visualize human tumor cell metastasis. Histochem Cell Biol. 2008; 130: 1119-1130.

22. Gabrielli MG, Accili D. The chick chorioallantoic membrane: a model of molecular, structural, and functional adaptation to transepithelial ion transport and barrier function during embryonic development. J Biomed Biotechnol. 2010; 2010: 940741.

23. Slodownik D, Grinberg I, Spira RM, Skornik Y, Goldstein RS. The human skin/chick chorioallantoic membrane model accurately predicts the potency of cosmetic allergens. Exp Dermatol. 2009; 18: 409-413.

24. Martinez-Madrid B, Donnez J, Van Eyck AS, Veiga-Lopez A, Dolmans MM, Van Langendonckt A. Chick embryo chorioallantoic membrane (CAM) model: a useful tool to study short-term transplantation of cryopreserved human ovarian tissue. Fertil Steril. 2009; 91: 285-292.

25. Nap AW, Groothuis PG, Punyadeera C, Klein-Hitpass L, Kamps R, Delvoux B, et al. Oral contraceptives prevent the development of endometriosis in the chicken chorioallantoic membrane model. Contraception. 2008; 78: 257-265.

26. Nap AW, Groothuis PG, Punyadeera C, Klein-Hitpass L, Kamps R, Delvoux B, et al. Oral contraceptives prevent the development of endometriosis in the chicken chorioallantoic membrane model. Contraception. 2008; 78: 257-265.

27. Larger E, Marre M, Corvol P, Gasc JM. Hyperglycemia-induced defects in angiogenesis in the chicken chorioallantoic membrane model. Diabetes. 2004; 53: 752-761.

28. Chin WW, Heng PW, Lim PL, Lau WK, Olivo M. Membrane transport enhancement of chlorin e6-polyvinylpyrrolidone and its photodynamic efficacy on the chick chorioallantoic model. J Biophotonics. 2008; 1: 395-407.

29. Clancy AA, Gregoriou Y, Yaehne K, Cramb DT. Measuring properties of nanoparticles in embryonic blood vessels: Towards a physicochemical basis for nanotoxicity. Chemical Physics Letters. 2010; 488: 99-111.

30. Yaehne K, Tekrony A, Clancy A, Gregoriou Y, Walker J, Dean K, et al. Nanoparticle accumulation in angiogenic tissues: towards predictable pharmacokinetics. Small. 2013; 9: 3118-3127.

31. Yaehne K, Tekrony, A., Clancy, A., Gregoriou, Y., Walker, J.T., Dean, K., Nguyen, T., Doiron, A., Rinker, K., Jiang, S., Childs, S., and Cramb, D. Nanoparticle Accumulation in Angiogenic Tissues: Towards Predictable Pharmacokinetics. Accepted, Small. 2013.

32. Diaspro A, Chirico G, Collini M. Two-photon fluorescence excitation and related techniques in biological microscopy. Q Rev Biophys. 2005; 38: 97-166.

33. Stober W, Fink A, Bohn E. Controlled growth of monodisperse silica spheres in the micron size range. J Colloid Interface Sci. 1968; 26:62-69.

34. Larson DR, Ow H, Vishwasrao HD, Heikal AA, Wiesner U, Webb WW. Silica Nanoparticle Architecture Determines Radiative Properties of Encapsulated Fluorophores. Chem Mater. 2008; 20: 2677-2684.

35. West LJ. Research Proposal: Nanomedicine in Organ Transplantation: Polysaccharide Structures as Immunologic Tolerogens for Infant Heart Transplantation. Edmonton, AB: University of Alberta, 2008.

36. Goyan R, Paul R, Cramb DT. Photodynamics of latex nanospheres examined using two-photon fluorescence correlation spectroscopy. J Phys Chem B. 2001; 105: 2322-2330.

37. Schwille P, Haustein, E. Fluorescence Correlation Spectroscopy, An Introduction to its Concepts and Applications. In: Schwille P, editor. Single Molecule Techniques: Biophysical Society; 2002.

38. Samkoe KS, Cramb DT. Application of an ex ovo chicken chorioallantoic membrane model for two-photon excitation photodynamic therapy of age-related macular degeneration. J Biomed Opt. 2003; 8: 410-417.

39. Eberbeck D, Wiekhorst F, Steinhoff U, Trahms L. Aggregation behaviour of magnetic nanoparticle suspensions investigated by magnetorelaxometry. J Phys: Condens Matter. 2006; 18: S2829.

40. Maldiney T, Richard C, Seguin J, Wattier N, Bessodes M, Scherman D. Effect of Core Diameter, Surface Coating, and PEG Chain Length on the Biodistribution of Persistent Luminescence Nanoparticles in Mice. ACS Nano. 2011; 5: 854-862.

41. Janković BD, Isaković K, Lukić ML, Vujanović NL, Petrović S, Marković BM.. Immunological capacity of the chicken embryo. I. Relationship between the maturation of lymphoid tissues and the occurrence of cell-mediated immunity in the developing chicken embryo. Immunology. 1975; 29: 497-508.

42. Arnida, Janát-Amsbury MM, Ray A, Peterson CM, Ghandehari H. Geometry and surface characteristics of gold nanoparticles influence their biodistribution and uptake by macrophages. Eur J Pharm Biopharm. 2011; 77: 417-423.

43. Avgoustakis K, Beletsi A, Panagi Z, Klepetsanis P, Livaniou E, Evangelatos G, et al. Effect of copolymer composition on the physicochemical characteristics, in vitro stability, and biodistribution of PLGA-mPEG nanoparticles. Int J Pharm. 2003; 259: 115-127.

44. Ishihara T, Maeda T, Sakamoto H, Takasaki N, Shigyo M, Ishida T, et al. Evasion of the accelerated blood clearance phenomenon by coating of nanoparticles with various hydrophilic polymers. Biomacromolecules. 2010; 11: 2700-2706.

45. Wang M, Thanou M. Targeting nanoparticles to cancer. Pharmacol Res. 2010; 62: 90-99.

Austin J Nanomed Nanotechnol - Volume 1 Issue 1 - 2013
ISSN : 2381-8956 | www.austinpublishinggroup.org

Citation: Cramb D , Wright V, Slaney A, Al-Atar U, Frederick A, et al. Long Circulating Nanoparticles as Potential Antigen Carriers in Angiogenic Blood Vessels: Towards Tolerogenesis. Austin J Nanomed Nanotechnol. 2013;1(1): 1005.